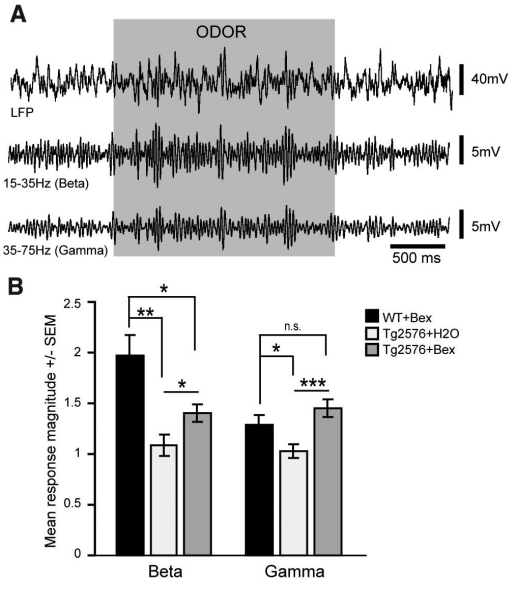

Fig. 4. Rescue of cortical network activity with bexarotene. LFP recordings of Tg2576 or nontransgenic (NonTg) mice (12 to 14 months) gavaged with bexarotene (Bex) (100 mg kg^{-1} day^{-1}) or vehicle (H_2O) for 3 days after implantation of electrodes into PCX. PCX LFPs in response to the odor ethyl valerate in an awake nontransgenic, bexarotene-treated mouse. (**A**) Fifteen- to 35-Hz beta- and 35- to 75-Hz gamma-band power traces (second-order band pass). (**B**) PCX odor-evoked response magnitudes (2 s odor/2 s pre-odor) ($n = 5$ mice per group, four odor presentations per mouse; $^*P < 0.05$, $^{**}P < 0.01$, $^{***}P < 0.001$, mean ± SEM, two-tailed t tests of mean odor-evoked magnitudes within LFP bins). ns, not significant.

can be improved through reducing brain-soluble Aβ levels, either upon the administration of ß- or γ-secretase inhibitors (*20*, *21*) or provision of antibodies against Aβ (*22*). However, the behavioral improvements were poorly correlated with the microglial-mediated removal of insoluble, deposited forms of Aβ. The dual actions of the nuclear receptors resulting in the enhanced expression and lipidation of apoE and modulation of the microglial-mediated immune response are consistent with recent genetic association analyses implicating them in the etiology of AD (*23*–*25*). The ability of bexarotene to rapidly reverse a broad range of deficits suggests that RXR agonists may be of therapeutic utility in the treatment of AD and its antecedent phases.

References and Notes

1. H. W. Querfurth, F. M. LaFerla, *N. Engl. J. Med.* **362**, 329 (2010).
2. K. G. Mawuenyega *et al.*, *Science* **330**, 1774 (2010).
3. J. J. Palop, L. Mucke, *Nat. Neurosci.* **13**, 812 (2010).
4. A. D. Roses, A. M. Saunders, *Curr. Opin. Biotechnol.* **5**, 663 (1994).
5. J. J. Donkin *et al.*, *J. Biol. Chem.* **285**, 34144 (2010).
6. Q. Jiang *et al.*, *Neuron* **58**, 681 (2008).
7. A. Chawla *et al.*, *Mol. Cell* **7**, 161 (2001).
8. P. Lefebvre, Y. Benomar, B. Staels, *Trends Endocrinol. Metab.* **21**, 676 (2010).
9. J. I. Odegaard, A. Chawla, *Annu. Rev. Pathol.* **6**, 275 (2011).
10. S. Mandrekar-Colucci, G. E. Landreth, *Expert Opin. Ther. Targets* **15**, 1085 (2011).
11. FDA, www.accessdata.fda.gov/drugsatfda_docs/nda/99/21055_Targretin.cfm (1999).
12. L. T. Farol, K. B. Hymes, *Expert Rev. Anticancer Ther.* **4**, 180 (2004).
13. J. R. Cirrito *et al.*, *J. Neurosci.* **23**, 8844 (2003).
14. R. Radde *et al.*, *EMBO Rep.* **7**, 940 (2006).
15. D. W. Wesson, D. A. Wilson, *Behav. Brain Res.* **216**, 408 (2011).
16. C. Murphy, *Physiol. Behav.* **66**, 177 (1999).
17. D. W. Wesson, E. Levy, R. A. Nixon, D. A. Wilson, *J. Neurosci.* **30**, 505 (2010).
18. D. W. Wesson *et al.*, *J. Neurosci.* **31**, 15962 (2011).
19. N. Kopell, G. B. Ermentrout, M. A. Whittington, R. D. Traub, *Proc. Natl. Acad. Sci. U.S.A.* **97**, 1867 (2000).
20. H. Fukumoto *et al.*, *J. Neurosci.* **30**, 11157 (2010).
21. T. A. Comery *et al.*, *J. Neurosci.* **25**, 8898 (2005).
22. J. C. Dodart *et al.*, *Nat. Neurosci.* **5**, 452 (2002).
23. L. Jones *et al.*, *PLoS ONE* **5**, e13950 (2010).
24. P. Hollingworth *et al.*, *Nat. Genet.* **43**, 429 (2011).
25. A. C. Naj *et al.*, *Nat. Genet.* **43**, 436 (2011).

Acknowledgments: We thank Dr. Mangelsdorf for discussions and M. Pendergast, G. Casadesus, and I. Nagle for technical assistance. This work was supported by the Blanchette Hooker Rockefeller Foundation, Thome Foundation, Roby and Taft Funds for Alzheimer's Research, Painstone Foundation, American Health Assistance Foundation, Cure Alzheimer's Fund, Coins for Alzheimer's Research Trust, and the National Institute on Aging (NIA) (grant AG030482-03S1 to G.E.L.); National Institute on Deafness and Other Communication Disorders (grant DC003906, RO1-AG037693 to D.A.W); NIA (grants K01 AG029524 and P50-AG005681), Shmerler family, and the Charles F. and Joanne Knight Alzheimer's Disease Research Center at Washington University (to J.R.C.); and Marian S. Ware Alzheimer Program (to K.R.B.). All raw data are archived on \\gel-server1 for authorized users. P.E.C. and G.E.L. hold U.S. Provisional Patent Application no. 61/224,709 regarding bexarotene as a potential therapeutic for Alzheimer's disease and are founding scientists of ReXceptor, Inc., which has licensing options from Case Western Reserve University on the use of bexarotene in the treatment of Alzheimer's disease.

Supporting Online Material

www.sciencemag.org/cgi/content/full/science.1217697/DC1
Materials and Methods
Figs. S1 to S7
References (*26*–*31*)

9 December 2011; accepted 20 January 2012
Published online 9 February 2012;
10.1126/science.1217697

Long-Range–Projecting GABAergic Neurons Modulate Inhibition in Hippocampus and Entorhinal Cortex

Sarah Melzer,[1]* Magdalena Michael,[1]* Antonio Caputi,[1]* Marina Eliava,[1] Elke C. Fuchs,[1] Miles A. Whittington,[2] Hannah Monyer[1]†

The hippocampus and entorhinal cortex play a pivotal role in spatial learning and memory. The two forebrain regions are highly interconnected via excitatory pathways. Using optogenetic tools, we identified and characterized long-range γ-aminobutyric acid–releasing (GABAergic) neurons that provide a bidirectional hippocampal-entorhinal inhibitory connectivity and preferentially target GABAergic interneurons. Activation of long-range GABAergic axons enhances sub- and suprathreshold rhythmic theta activity of postsynaptic neurons in the target areas.

The excitatory projections connecting the hippocampus and entorhinal cortex (*1*) account for the functional interdependence of these two brain regions (*2*–*4*). Excitatory neurons in the hippocampus and entorhinal cortex are under control of local γ-aminobutyric acid–releasing (GABAergic) interneurons (*5*, *6*). Some GABAergic neurons also project long distance. For example, long-range–projecting GABAergic cells connect hippocampus with medial septum (*7*–*9*) and other extra-hippocampal brain areas (*10*, *11*), suggesting that interregional GABAergic connectivity might be less rare than was previously assumed (*12*).

To test for the presence of hippocampal GABAergic neurons projecting to the medial enthorinal cortex (MEC), we injected the retrograde tracer fluorogold (FG) into the MEC of wild-type mice (fig. S1). In addition to the expected labeling of numerous excitatory cells, we found FG^+ neurons in stratum oriens and stratum radiatum of CA1 and in the hilus of the dentate gyrus (DG), indicating retrogradely labeled GABAergic cells. We detected FG-labeled cells coexpressing somatostatin (SOM) in stratum oriens of CA1 (23 cells, nine mice) and also in the hilus of the DG (14 cells, nine mice) (Fig. 1, A and B).

[1]Department of Clinical Neurobiology of the Medical Faculty of Heidelberg University and German Cancer Research Center (DKFZ), Im Neuenheimer Feld 280, 69120 Heidelberg, Germany. [2]Institute of Neurosciences, The Medical School, Newcastle University, Framlington Place, Newcastle, NE2 4HH, UK.

*These authors contributed equally to this work.
†To whom correspondence should be addressed. E-mail: h.monyer@dkfz-heidelberg.de

To provide direct evidence for the presence of hippocampal SOM$^+$ neurons projecting to the MEC, we injected the adeno-associated viral (AAV) vector AAV DIO *ChR2-mCherry* (*13*) into the dorsal hippocampus of *SOM^{Cre}* mice (Fig. 1C and fig. S2), achieving specific expression of the fluorescent fusion protein ChR2-mCherry in SOM$^+$ neurons (Fig. 1C). We detected mCherry-labeled axons of SOM$^+$ hippocampal neurons in the medial septum and the contralateral DG (Fig. 1D) (*14*, *15*). We also detected labeled axons originating from hippocampal SOM$^+$ neurons in the striatum (fig. S3) and MEC (Fig. 1E). In the MEC, long-range–projecting axons crossed orthogonally from layer VI (LVI) to LII, branched in the

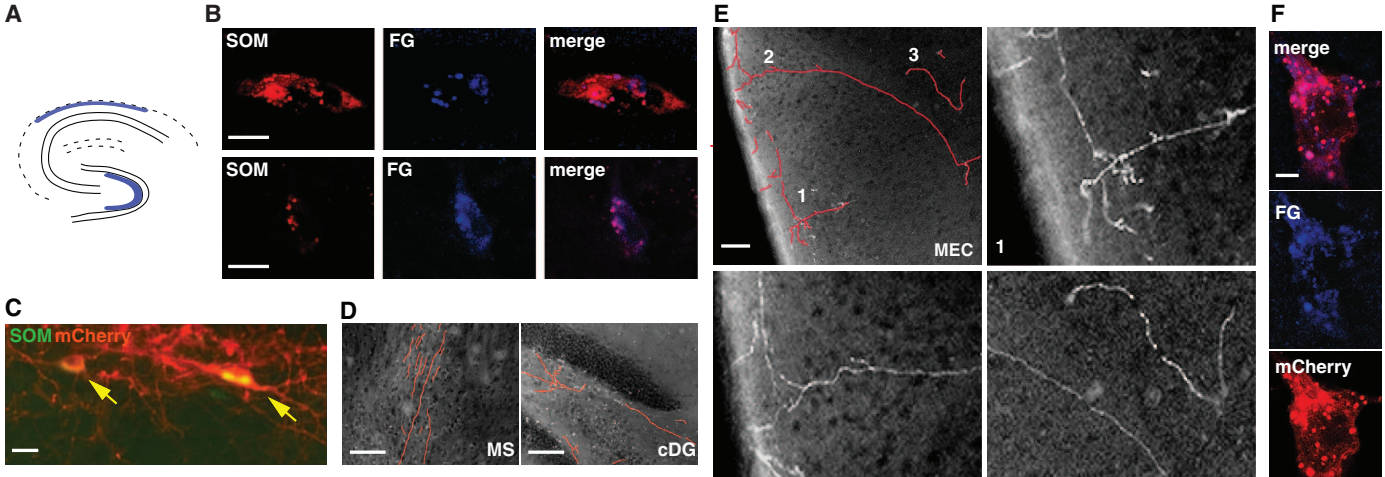

Fig. 1. Long-range–projecting hippocampal SOM$^+$ neurons target superficial layers in the MEC. (**A**) Schematic drawing showing the location of retrogradely labeled SOM$^+$ cells in CA1 and DG of the dorsal hippocampus after FG injection into the MEC. (**B**) Confocal images of a SOM$^+$/FG–labeled neuron in stratum oriens of CA1 (top row) and the hilus of the DG (bottom row). Scale bar, 10 μm. (**C**) Coexpression of SOM and ChR2-mCherry in CA1 stratum oriens after virus injection into the dorsal hippocampus in a *SOM^{Cre}* mouse. ChR2-mCherry expression was restricted to SOM$^+$ cells (yellow arrows). Scale bar, 30 μm. (**D**) Digitally encoded (red) mCherry$^+$ axons of long-range–projecting hippocampal SOM$^+$ cells detected in medial septum (MS, left) and contralateral DG (right). Scale bar, 100 μm. (**E**) Digitally encoded (red) mCherry$^+$ axons of long-range–projecting hippocampal SOM$^+$ cells in the MEC. Projections indicated by numbers are shown as higher magnification. Scale bar, 150 μm. (**F**) Confocal images of a mCherry and FG double-labeled cell in stratum oriens of the CA1 region after virus injection into dorsal hippocampus and FG injection into the MEC. Scale bar, 10 μm.

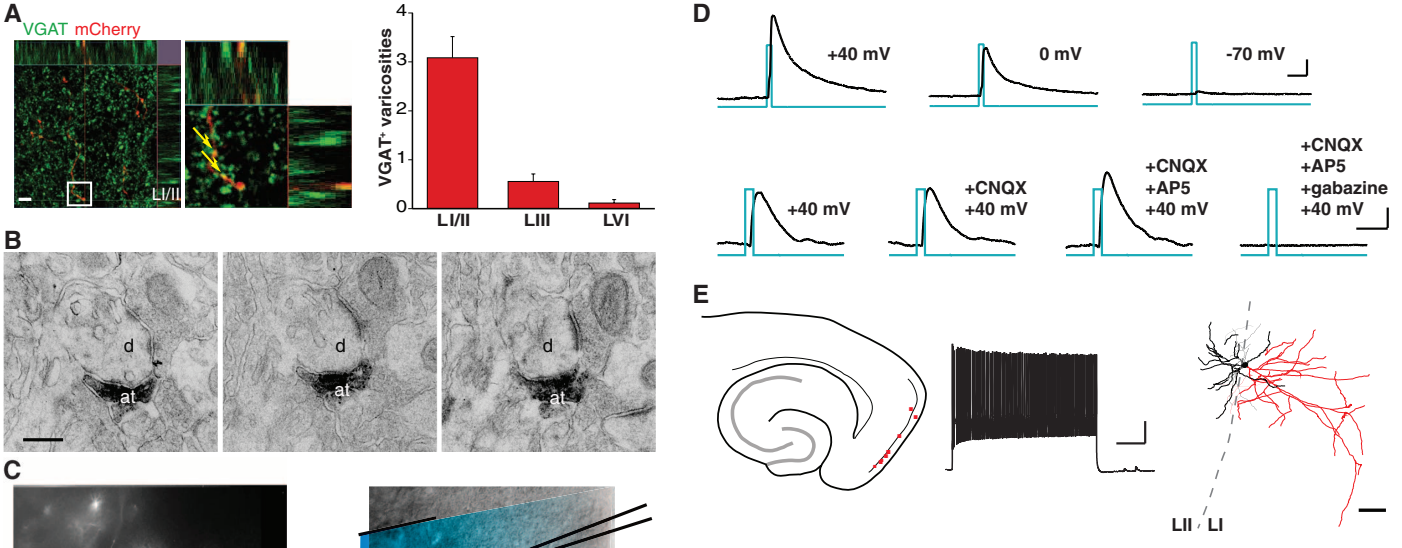

Fig. 2. Hippocampal SOM$^+$-projecting neurons form inhibitory synapses onto GABAergic neurons in the MEC. (**A**) VGAT$^+$ varicosities (arrows) of mCherry-labeled long-range projections in layer I/II of the MEC (left) and quantification in the indicated layers of the MEC. (Right) Bar histogram representing average number of VGAT$^+$ varicosities (60 optical sections, 2500 μm^2 each, mean ± SEM; five hemispheres of three mice). Scale bar, 5 μm. (**B**) Electronmicrographs showing serial sections of an immunogold-labeled ChR2-mCherry–expressing axon terminal (at) that forms a symmetric synapse onto a dendrite (d). Scale bar, 0.25 μm. (**C**) Fluorescence image of mCherry-labeled axons in the MEC (left). Asterisk indicates the location of a target cell shown in the DIC image (right). Presynaptic axon was stimulated with blue laser light, and PSCs were recorded in the target cell. Scale bar, 25 μm. (**D**) Inhibitory PSCs recorded in a target cell at indicated holding potentials. Responses could be blocked by gabazine but not CNQX and AP5. Scale bars, 20 ms and 50 pA. (**E**) Schematic drawing of a horizontal section showing the location of target neurons (red dots) that were biocytin-filled for subsequent reconstruction (left). Firing pattern most frequently found in MEC target cells (middle). Scale bars, 200 ms and 20 mV. (Right) A representative reconstructed target cell (dendrites, black; axon, red). Scale bar, 100 μm.

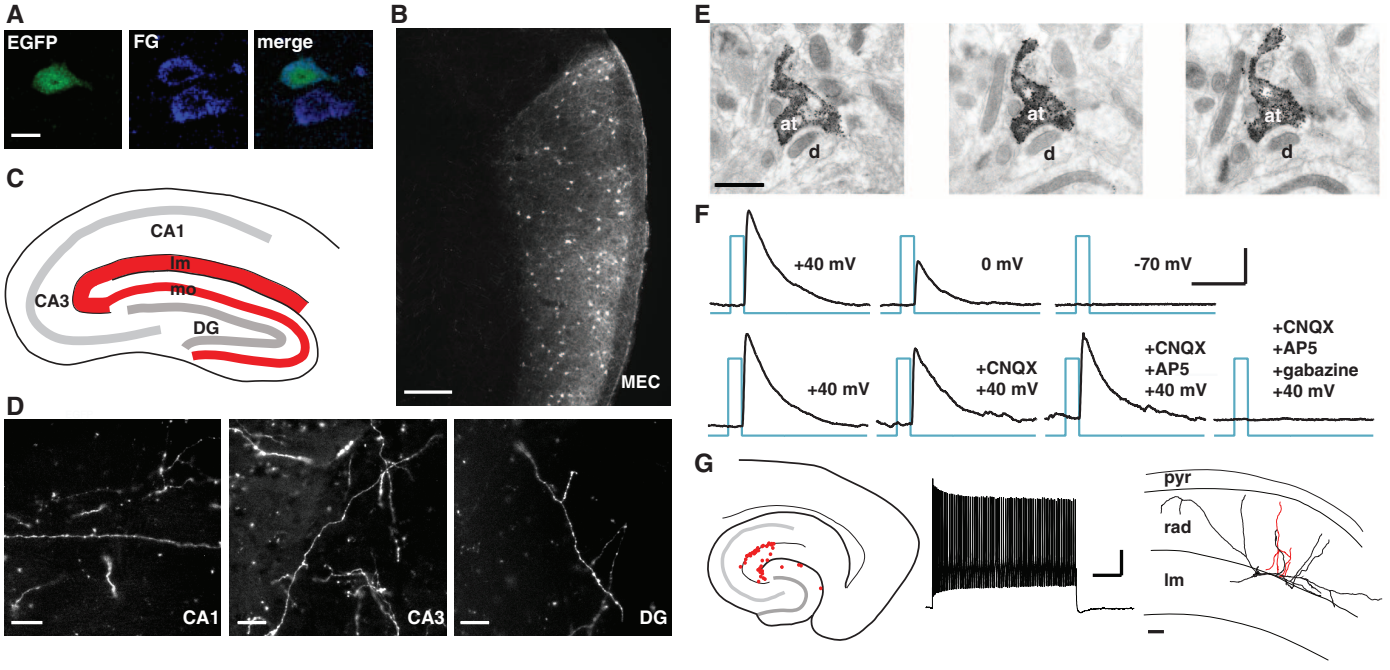

Fig. 3. MEC long-range GABAergic neurons form functional synapses onto GABAergic neurons in the hippocampus. (**A**) Retrogradely labeled GABAergic cell in the MEC after FG injection into the dorsal hippocampus of a *GAD67*^{EGFP} mouse. Scale bar, 10 μm. (**B**) mCherry expression in MEC GABAergic cells subsequent to AAV DIO *ChR2-mCherry* injection into a *GAD*^{Cre} mouse. Scale bar, 500 μm. (**C**) Schematic drawing of a sagittal hippocampal section indicating areas targeted by long-range–projecting MEC GABAergic neurons (red). (**D**) Fluorescent axons are located in stratum lacunosum-moleculare (lm) of the CA1 and CA3 areas and in stratum moleculare (mo) of the DG. Scale bars, 25 μm (CA1) and 12.5 μM (CA3 and DG). (**E**) Electronmicrographs showing serial sections of an immunogold-labeled ChR2-mCherry–expressing axon terminal (at) that forms a symmetric synapse onto a dendrite (d). Scale bar, 0.5 μm. (**F**) Inhibitory PSCs recorded in a target cell in stratum lacunosum-moleculare at indicated holding potentials. Response was blocked by gabazine but not CNQX or AP5. Scale bars, 20 ms and 50 pA. (**G**) Schematic drawing of a horizontal section of the intermediate hippocampus indicating the location of responsive target cells (red dots). Firing pattern most frequently found in hippocampal target cells (middle). Scale bars, 200 ms and 20 mV. (Right) Corresponding reconstruction in a sagittal section. Scale bar, 100 μm.

transition zone between LII and LI, and extended horizontally within LI over a distance of up to several 100 μm (Fig. 1E). We usually observed one to three projections per 50-μm section. Combining virus injection into the dorsal hippocampus with retrograde tracer injection into the MEC, we found individual CA1 neurons that were co-labeled with mCherry and FG (Fig. 1F). The population of hippocampal SOM$^+$ long-range–projecting neurons targeting the MEC appears to be distinct from the one projecting to the medial septum (fig. S4).

Using immmunohistochemistry, electron microscopy (EM), and whole-cell patch-clamp recordings, we subsequently investigated whether long-range–projecting hippocampal SOM$^+$ neurons form inhibitory synapses in the MEC. The mCherry-labeled axons were VGAT$^+$ and VGluT1-negative (Fig. 2A) and established symmetric synapses in LI and LII (Fig. 2B). We tested for functional synapses by laser-stimulating ChR2-mCherry–expressing terminals and recording from putative postsynaptic cells located in the vicinity of the labeled axons (Fig. 2C). Responses could be detected in 60 out of 686 patched cells (n = 41 mice). At +40 mV, the mean amplitude of the postsynaptic currents (PSCs) was 84.15 ± 11.94 pA, and the mean latency was 3.13 ± 0.22 ms (n = 37 cells). PSCs were inhibitory, as indicated by the reversal potential (~–70 mV, n = 25 out of 25 cells), the pharmacological block of the responses by the GABA type A ($GABA_A$) receptor antagonist gabazine (n = 17 out of 17 cells), and the lack of effect using the glutamatergic blockers 6-cyano-7-nitroquinoxaline-2,3-dione (CNQX) and (2*R*)-amino-5-phosphonovaleric acid (AP5) (n = 3 out of 3 cells) (Fig. 2D). All target cells identified through whole-cell recording were located close to or at the transition zone between LI and LII (Fig. 2E and fig. S5).

Hippocampal SOM$^+$ long-range–projecting neurons preferentially targeted GABAergic interneurons in the MEC. On the basis of their firing pattern, out of 20 target cells 16 could be classified as interneurons and 4 as stellate cells. The firing pattern of the interneurons was not uniform, indicating that they comprised different subtypes (fig. S6). Biocytin-filling revealed that axons of target cells arborized mainly in LI (n = 6 cells, three mice) (Fig. 2E).

FG injection into the MEC suggested that in addition to SOM$^+$ cells, other hippocampal GABAergic neurons project to the MEC (fig. S1B). AAV DIO *ChR2-mCherry* injection into the dorsal hippocampus of *GAD*^{Cre} mice (*16*) resulted in a larger number of labeled long-range–projecting axons that were VGAT$^+$ and covered additional target fields in the MEC (such as the presence of branches also in deeper layers) (fig. S7). Nineteen target cells were identified upon laser stimulation, and when tested, on the basis of the firing pattern all target cells were GABAergic (n = 12 out of 12 cells).

Retrograde labeling experiments have indicated the presence of long-range–projecting GABAergic cells in the opposite direction, from the entorhinal cortex to the hippocampus (*17*). When dorsal hippocampi of *GAD67*^{EGFP} mice were FG-injected, we detected FG/enhanced green fluorescent protein (EGFP) double-labeled cells in LII and LIII of the MEC (10 out of 1147 FG$^+$ cells counted, n = 5 mice) (Fig. 3A). We therefore injected AAV DIO *ChR2-mCherry* into the MEC of *GAD*^{Cre} mice (Fig. 3B) and readily detected mCherry-labeled axons in stratum lacunosum-moleculare/radiatum of the hippocampal CA areas, and stratum moleculare of the DG (Fig. 3, C and D).

We also analyzed the entorhinal-hippocampal connections anatomically and functionally. Fluorescently labeled long-range axons were VGAT$^+$ (fig. S8), and EM analysis of labeled axons in stratum lacunosum-moleculare/radiatum (n = 6 mice) showed that long-range projections formed symmetric synapses (Fig. 3E). Laser stimulation of presynaptic ChR2-expressing long-range projections allowed the identification of 86 responding target cells (out of ~1000 patched neurons from 65 mice) (mean amplitude and latency of PSCs at +40 mV was 101.45 ± 22.75 pA and 4.47 ± 0.50 ms, respectively; n = 19 cells) (Fig. 3F).

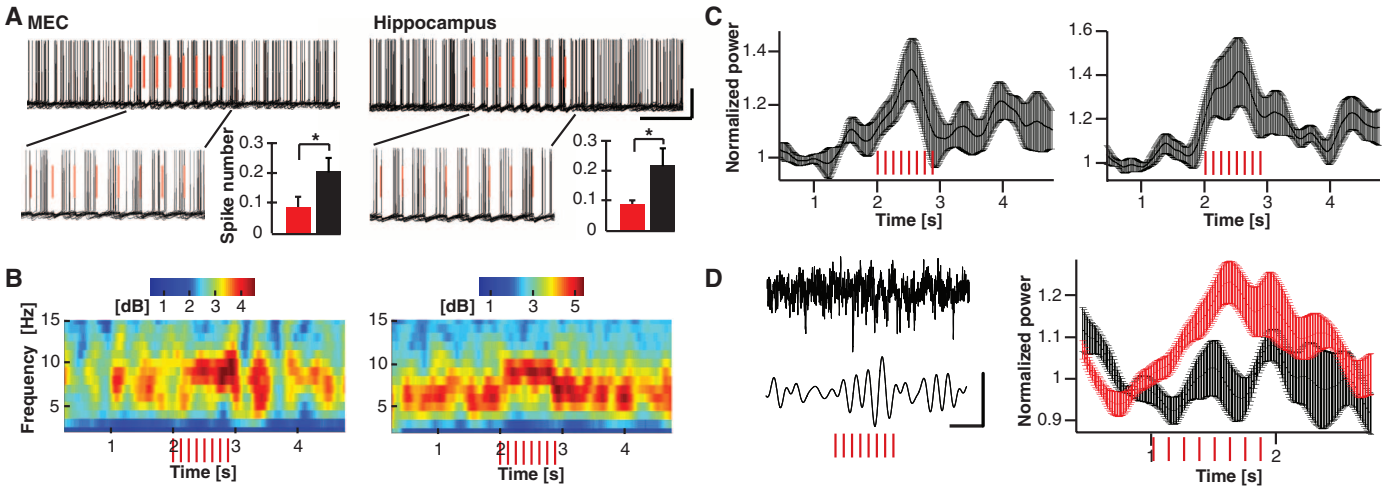

Fig. 4. Activation of GABAergic long-range projections enhances rhythmic activity in the MEC and the hippocampus. MEC target cells in hippocampal AAV DIO *ChR2-mCherry*–injected *SOM*^{Cre} mice [(A) to (C), left] and hippocampal target cells in MEC AAV DIO *ChR2-mCherry*–injected *GAD*^{Cre} mice [(A) to (C), right] cells were patched and depolarized to suprathreshold potentials. Long-range projections were stimulated at 8 Hz (red ticks). (**A**) Overlay of 20 unfiltered traces recorded in a target cell, with indicated enlargement of action potential firing during the stimulation period. Scale bars, 40 mV and 500 ms. Histogram below indicates mean number of spikes ± SEM within the first 62.5-ms interval directly after laser stimulation (red bar) and the subsequent 62.5-ms interval (black bar). (**B**) Spectrogram showing that activation of long-range–projecting axons entrains target cell to fire rhythmically at theta range frequency. (**C**) Increase in theta power (7 to 9 Hz) in target cells during laser stimulation. (**D**) Representative unfiltered (top) and filtered (3 to 7 Hz, bottom) trace of DHPG/NBQX–induced CA1 theta oscillations. (Right) Averaged power of 3- to 7-Hz oscillations normalized to power before stimulation for wild-type (black) and *GAD*^{Cre}-injected mice (red). Scale bars, 500 ms and 0.1 mV.

The GABAergic nature of these synapses was also confirmed by the reversal potential (n = 12 out of 12 cells) and selective gabazine blockage (n = 17 out of 17 cells). All detected target cells were located in dorsal and intermediate hippocampal areas that are known to contain interneurons only—namely, stratum lacunosum-moleculare and deep stratum radiatum in all CA areas and in stratum moleculare of the DG (Fig. 3G). In more than 110 pyramidal and granule cells that were patched, no PSCs could be detected, suggesting a preferential, if not even exclusive, targeting of GABAergic interneurons. The firing pattern (n = 26 cells) (Fig. 3G and fig. S9) and morphology (n = 19 cells) (Fig. 3G) of the target cells confirmed their interneuronal phenotype.

To establish the immunochemical identity of MEC GABAergic projection neurons, we combined FG retrograde labeling and immunohistochemistry, using different interneuron markers. FG/EGFP double-labeling in the MEC was found in a subpopulation of parvalbumin^{+} (PV) neurons (fig. S10A) and in additional GABAergic neurons of unknown immunochemical identity. Injection of AAV DIO *ChR2-mCherry* into the MEC of *PV*^{Cre} (*18*) mice further substantiated the finding that MEC PV^{+} cells projected to the hippocampus (fig. S10B) and formed functional synapses on hippocampal interneurons (n = 5 electrophysiologically identified target cells in CA1-3 and DG) (fig. S10, C and D).

To directly investigate whether long-range GABAergic cells modulate the activity of targeted cells, we recorded sub- and suprathreshold activity in targeted interneurons in slices of the MEC and the hippocampus during stimulation of long-range–projecting axons. Laser stimulation at 8 Hz for 1 s enhanced rhythmic firing of the postsynaptic neuron, as indicated by the reduction of the action potential number during the first half of each 125-ms-pulse interval in target cells in the MEC (n = 5 cells, P = 0.03) and in the hippocampus (n = 6 cells, P = 0.02) (Fig. 4A). Thus, axonal stimulation resulted in an increase in rhythmicity in theta range, as shown by the spectrogram of individual neurons (Fig. 4B) and the comparison of theta power during and before stimulation (n = 5 and 6 and P = 0.03 and 0.02 for MEC and hippocampus target cells, respectively) (Fig. 4C). There was no significant difference in the overall firing rate before, during, and after stimulation (fig. S11A). Axonal stimulation at 40 Hz frequency did not affect rhythmic firing of target cells (n = 7 and 5 for MEC and hippocampus, respectively) (fig. S11, B and C). Axonal stimulation at 8 Hz also increased subthreshold oscillations at theta frequency (n = 10 and 7 and P = 0.0002 and 0.02 for MEC and hippocampus target cells, respectively) (fig. S11, D to G).

Last, because theta oscillations can be induced pharmacologically in acute hippocampal slices (*19*) we analyzed whether recruitment of long-range GABAergic cells affected network activity. We recorded (*S*)-3,5-dihydroxyphenylglycine (DHPG)/2,3-dihydroxy-6-nitro-7-sulfamoyl-benzo[f]quinoxaline-2,3-dione (NBQX)–induced theta oscillations in the CA1 region. Hippocampal 8-Hz laser stimulation of MEC-derived axons increased theta power (3 to 7 Hz) significantly in slices obtained from MEC virus-injected *GAD*^{Cre} (n = 14 slices, $P < 0.05$) but not wild-type mice (n = 7 slices, $P > 0.1$) (Fig. 4D). Stimulation at 40 Hz did not change gamma power (n = 12 slices) (fig. S11H).

Using optogenetic viral tracing, we identified long-range GABAergic neurons connecting the hippocampus and the MEC. Furthermore, we provided functional evidence that long-range GABAergic neurons target local interneurons whose activity they modulate. It has been postulated that long-range–projecting GABAergic neurons might be an ideal substrate to precisely coordinate activity between distant brain regions (*20*). Long-range GABAergic neurons in the hippocampal-entorhinal formation might well account for the highly synchronized theta activity in the hippocampus and entorhinal cortex (*21*) and thus contribute to the proposed mechanisms underlying spatial and temporal coding and ultimately spatial memory (*22*, *23*).

References and Notes

1. C. B. Canto, F. G. Wouterlood, M. P. Witter, *Neural Plast.* **2008**, 1 (2008).
2. A. Bragin *et al.*, *J. Neurosci.* **15**, 47 (1995).
3. V. H. Brun *et al.*, *Neuron* **57**, 290 (2008).
4. A. Ylinen *et al.*, *Hippocampus* **5**, 78 (1995).
5. T. Klausberger, P. Somogyi, *Science* **321**, 53 (2008).
6. R. D. Traub, A. Bibbig, F. E. LeBeau, E. H. Buhl, M. A. Whittington, *Annu. Rev. Neurosci.* **27**, 247 (2004).
7. T. F. Freund, M. Antal, *Nature* **336**, 170 (1988).
8. V. T. Takács, T. F. Freund, A. I. Gulyás, *Eur. J. Neurosci.* **28**, 148 (2008).
9. K. Tóth, Z. Borhegyi, T. F. Freund, *J. Neurosci.* **13**, 3712 (1993).
10. S. Jinno *et al.*, *J. Neurosci.* **27**, 8790 (2007).
11. J. Apergis-Schoute, A. Pinto, D. Paré, *J. Neurosci.* **27**, 4061 (2007).
12. N. Tamamaki, R. Tomioka, *Front. Neurosci.* **4**, 202 (2010).

13. J. A. Cardin *et al.*, *Nat. Protoc.* **5**, 247 (2010).
14. S. Jinno, T. Kosaka, *Brain Res.* **945**, 219 (2002).
15. C. A. Zappone, R. S. Sloviter, *J. Comp. Neurol.* **441**, 324 (2001).
16. S. Tolu *et al.*, *FASEB J.* **24**, 723 (2010).
17. P. Germroth, W. K. Schwerdtfeger, E. H. Buhl, *Brain Res.* **494**, 187 (1989).
18. E. C. Fuchs *et al.*, *Neuron* **53**, 591 (2007).
19. M. J. Gillies *et al.*, *J. Physiol.* **543**, 779 (2002).
20. G. Buzsáki, J. J. Chrobak, *Curr. Opin. Neurobiol.* **5**, 504 (1995).
21. K. Mizuseki, A. Sirota, E. Pastalkova, G. Buzsáki, *Neuron* **64**, 267 (2009).
22. J. O'Keefe, L. Nadel, *The Hippocampus as a Cognitive Map* (Oxford Univ Press, Oxford, 1978).
23. M. P. Witter, E. I. Moser, *Trends Neurosci.* **29**, 671 (2006).

Acknowledgments: We thank K. Deisseroth for the AAVs, A. Vogt for help in generating mice, I. Preugschat-Gumprecht and R. Hinz for their technical assistance, and P. H. Seeburg for helpful discussions. This work was supported by a European Research Council grant (GABAcellsAndMemory grant 250047, to H.M.) and a German Ministry of Education and Research (BMBF) grant 01GQ1003A to H.M. and E.C.F.

Supporting Online Material
www.sciencemag.org/cgi/content/full/335/6075/1506/DC1
Materials and Methods
Figs. S1 to S11
References

28 November 2011; accepted 10 February 2012
10.1126/science.1217139

Glucocorticoids Can Induce PTSD-Like Memory Impairments in Mice

Nadia Kaouane,[1,2,3] Yves Porte,[1,2]* Monique Vallée,[2,3] Laurent Brayda-Bruno,[1,2,3] Nicole Mons,[1,2]† Ludovic Calandreau,[4] Aline Marighetto,[1,2,3] Pier Vincenzo Piazza,[2,3]‡§ Aline Desmedt[1,2,3]‡§

Posttraumatic stress disorder (PTSD) is characterized by a hypermnesia of the trauma and by a memory impairment that decreases the ability to restrict fear to the appropriate context. Infusion of glucocorticoids in the hippocampus after fear conditioning induces PTSD-like memory impairments and an altered pattern of neural activation in the hippocampal-amygdalar circuit. Mice become unable to identify the context as the correct predictor of the threat and show fear responses to a discrete cue not predicting the threat in normal conditions. These data demonstrate PTSD-like memory impairments in rodents and identify a potential pathophysiological mechanism of this condition.

Situations surrounding threatening events are better remembered than the ones accompanying neutral ones. This hypermnesia for environments and cues predicting threats is important for adaptation because it increases the probability of survival in uncontrolled environments. In humans, the exposure to threatening situations can also result in memory impairments culminating in severe pathological states such as posttraumatic stress disorder (PTSD) (*1*). In this case, a hypermnesia for the core traumatic event is associated with a memory deficit for peritraumatic contextual cues (*2*, *3*), impairing the capacity of the subject to identify the correct predictors of the threat and restrict fear to the correct place and/or to the correct cues. This deficit contributes to the intrusive recollection—re-experiencing the fear response in safe situations—that characterizes PTSD.

Animal models of traumatic memories and PTSD principally focus on the quantitative aspect of fear memories: an increased and persistent fear response (*4*). In contrast, the critical landmark of PTSD—the inability of the subject to restrict fear responses to the appropriate predictors—is largely neglected. As a consequence, the biological mechanisms of pathological PTSD-like memories remain largely unknown.

To address this issue, we analyzed whether PTSD-like memory impairments can be observed in mice. We therefore injected the stress hormone corticosterone, the major glucocorticoid in rodents, into the hippocampus of mice submitted to a fearful situation. Glucocorticoids increase in response to stress, enhance stress-related memories (*5*–*8*), and have been involved in the pathophysiology of PTSD (*9*, *10*). The hippocampus plays an important role in memory (*11*), is the major brain target of glucocorticoids (*12*, *13*), and seems impaired in PTSD (*14*, *15*).

We then developed a behavioral model that allows evaluating the ability of the individuals to restrict fear responses to the appropriate predictor of the threatening stimulus. Mice were first submitted to a threatening situation, the delivery of an electric footshock, when exposed to a discrete cue (a tone) in a specific context (conditioning cage). Twenty-four hours after this conditioning procedure, animals were re-exposed first to the cue alone in a familiar and safe environment and then to the conditioning context without the cue (*16*).

We used two distinct conditioning schedules that contained exactly the same nature and quantities of environmental stimuli but, differing in their associations, identified different predictors of the threat (*17*, *18*). In one schedule, the presentation of the tone was always followed by the delivery of the shock (predicting-cue group). In this case, animals identified the tone as the main predictor of the threat, showing conditioned fear when re-exposed to the cue alone but not to the context (Fig. 1A). During the second schedule, the tone presentation was never followed by the delivery of the shock (predicting-context group). In this case, animals identified the conditioning context as the correct predictor of the threat, showing conditioned fear when re-exposed to the context alone but not to the cue (Fig. 1A). As expected, in both conditions fear responses to the correct predictor progressively increased as a function of the threat intensity.

Corticosterone (10 ng per side) was infused into the dorsal hippocampus immediately after conditioning with three footshock intensities (0.3, 0.5, and 0.8 mA). In the predicting-cue group, corticosterone did not significantly modify fear responses (Fig. 1B). This is not surprising because the hippocampus is necessary for contextual conditioning but is dispensable for cue conditioning (*19*, *20*). In animals in which the context predicted the threat (predicting-context group), as expected (*6*, *7*) corticosterone administered after the lowest shock intensity (0.3 mA) enhanced conditioned fear to the context (Fig. 1B). However, when corticosterone followed the highest shock intensity (0.8 mA) PTSD-like memory impairments appeared. Animals did not show fear in response to the correct predictor of the threat, the context, but in response to the tone (Fig. 1B), which is normally not a relevant predictor of the threat for them. Animals infused with corticosterone also showed a fear response to a previously unexperienced cue (2 kHz tone) at some extent similar to the one (1 kHz tone) experienced during conditioning (Fig. 1C), but not in response to a completely different cue (white noise). In contrast, the fear response in the predicting-cue group was exclusively restricted to the conditioning cue. In conclusion, hippocampal corticosterone infusions impaired the ability of the subject to restrict fear responses to the appropriate predicting cues.

In physiological conditions, corticosterone increases systemically in response to stress. We then analyzed whether the exposure to a second stress, the restraint in a cylinder for 20 min, could also induce PTSD-like memory impairments. Similar to intrahippocampal corticosterone infusions, when the second stress followed the low shock intensity (0.3 mA) conditioned fear to the context

[1]CNRS UMR 5228, Centre de Neurosciences Intégratives et Cognitives, 33405 Talence, France. [2]Department of Life Science, Université de Bordeaux, 33077 Bordeaux, France. [3]INSERM U862, Neurocentre Magendie, 146 rue Leo Saignat, 33077 Bordeaux, France. [4]Institut National de la Recherche Agronomique (INRA) Centre de Tours Nouzilly, Physiologie de la Reproduction et des Comportements, CNRS UMR 6175, INRA UMR 85, Université de Tours–Haras Nationaux, 37380 Nouzilly, France.

*Present address: Institut des Maladies Neurodégénératives, CNRS UMR 5293, Universités Bordeaux 1 et 2, Avenue des Facultés, 33405 Talence, France.
†Present address: Institut de Neurosciences Cognitives et Intégratives d'Aquitaine, CNRS UMR 5287, Universités Bordeaux 1 et 2, Avenue des Facultés, 33405 Talence, France.
‡These authors contributed equally to this work.
§To whom correspondence should be addressed. E-mail: aline.desmedt@inserm.fr (A.D.); pier-vincenzo.piazza@inserm.fr (P.V.P.)

Long-Range–Projecting GABAergic Neurons Modulate Inhibition in Hippocampus and Entorhinal Cortex

Sarah Melzer, Magdalena Michael, Antonio Caputi, Marina Eliava, Elke C. Fuchs, Miles A. Whittington, and Hannah Monyer

Science, 335 (6075), • DOI: 10.1126/science.1217139

Inhibiting the Inhibitors

Excitatory neurons in the hippocampus and entorhinal cortex are under control of local #-aminobutyric acid–releasing (GABAergic) interneurons that are the major source of inhibition in the adult brain. In contrast to the wealth of knowledge regarding connectivity in the hippocampus, much less is known about the cross-talk between the hippocampus and other brain regions. Melzer *et al.* (p. 1506) investigated long-range GABAergic projections from the hippocampal formation to the medial entorhinal cortex and vice versa. These GABAergic neurons bidirectionally couple the hippocampus and medial entorhinal cortex and preferentially target local inhibitory neurons, forming disinhibitory loops that could help synchronize neuronal activity.